agriculture

MDPI

Article

Mass Spectrometry-Based Non-Targeted Lipidome Analysis and Extraction of Markers for the Authentication of White and Black Truffle Species and Their Origin Determination

Eva Tejedor-Calvo [1,2,*], Pedro Marco [1], Markus Fischer [3] and Marina Creydt [3,*]

[1] Department of Plant Science, Agrifood Research and Technology Centre of Aragon (CITA), Agrifood Institute of Aragón—IA2, CITA–Zaragoza University, Av. Montañana, 930, 50059 Zaragoza, Spain; pmarcomo@cita-aragon.es
[2] Laboratory for Aroma Analysis and Enology, Department of Analytical Chemistry, Faculty of Sciences, University of Zaragoza, 50009 Zaragoza, Spain
[3] Hamburg School of Food Science, Institute of Food Chemistry, University of Hamburg, Grindelallee 117, 20146 Hamburg, Germany; markus.fischer@uni-hamburg.de
* Correspondence: etejedor@unizar.es (E.T.-C.); marina.creydt@uni-hamburg.de (M.C.)

Abstract: The visual authentication of high-value truffles (*Tuber magnatum* and *Tuber melanosporum*) is challenging, as they share similar morphological characteristics with other truffle species that have a lower economic value. This similarity complicates accurate identification and increases the risk of substitution or mislabeling, which can affect both market prices and consumer trust. For this reason, the aim of this study was to apply a non-targeted lipidomic approach using ion mobility spectrometry-mass spectrometry to distinguish between white (*T. magnatum*, *Tuber borchii*, and *Tuber oligospermum*) and black truffle species (*T. melanosprum*, *T. aestivum*, *T. aestivum* var. *uncinatum*, *T. brumale*, and *T. indicum*) and to determine the different geographical origins of the two most valuable truffle species (*T. melanosporum* and *T. magnatum*). Among several hundred features, 37 and 57 lipids were identified as marker compounds to distinguish white and black truffle species using MS/MS spectra and collision cross section (CCS) values, respectively. Only a few marker compounds were necessary to recognize the differences between white and black truffles. In particular, ceramides, glycerolipids, and phospholipids proved to be particularly suitable for separating the species. In addition, different metabolite profiles were determined for *T. melanosporum* and *T. magnatum* depending on their geographical origin. These findings lay the groundwork for a comprehensive quality control framework for fresh truffles, ensuring authenticity, detecting adulteration, and preserving their premium status.

Keywords: truffles; lipids; omics; geographical origin; mass spectrometry; food fraud

check for updates

Citation: Tejedor-Calvo, E.; Marco, P.; Fischer, M.; Creydt, M. Mass Spectrometry-Based Non-Targeted Lipidome Analysis and Extraction of Markers for the Authentication of White and Black Truffle Species and Their Origin Determination. *Agriculture* **2024**, *14*, 2350. https://doi.org/10.3390/agriculture14122350

Academic Editor: Matteo Perini

Received: 19 November 2024
Revised: 15 December 2024
Accepted: 18 December 2024
Published: 20 December 2024

Copyright: © 2024 by the authors. Licensee MDPI, Basel, Switzerland. This article is an open access article distributed under the terms and conditions of the Creative Commons Attribution (CC BY) license (https://creativecommons.org/licenses/by/4.0/).

1. Introduction

The genus *Tuber*, belonging to the *Tuberaceae* family, includes approximately more than 180 species globally [1], but only a few of them are of gastronomic and economic interest [2]. Truffles can be classified as black or white truffles based on their peridium color (Table 1). Among them, *Tuber magnatum* (white truffle) and *Tuber melanosporum* (black truffle) are especially appreciated for their distinctive aroma [3,4], and they reach the highest prices (up to 4000 EUR/kg and 1500 EUR/kg, respectively) [5]). They are sometimes substituted with lower-value species due to their similar morphological characteristics. In the black category, it is included: *Tuber brumale* and *Tuber aestivum* (summer truffle) that are successfully cultivated [6] and traditionally harvested in Mediterranean countries, whereas *Tuber indicum* is exclusively harvested in Asia [2]. Also, the *T. aestivum* strain includes an ecotype commonly known as the Burgundy truffle (*T. aestivum* var. *uncinatum*) (from now on *T. uncinatum* in the text), which has a particularly intense aromatic profile [7]. In the white truffle category, *T. borchii* and *T. oligospermum* are included, among others.

Table 1. Truffle species selected for this study classified as black or white truffles depending on the peridium appearance.

Truffle Species	Other Names	Gleba Appearance	Peridium Appearance	Country	Harvest Season	References
Black truffles						
T. melanosporum	Périgord black, black truffle, and truffe noire	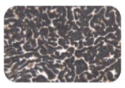		Native to the Mediterranean regions of Spain, France, Italy, and parts of Croatia and Serbia	Late November–early March	[8,9]
T. aestivum	Summer truffle			Northern Italy and parts of France	September–December	[8,9]
T. aestivum var. *uncinatum*	Autum truffle			Northern Italy and parts of France	September–December	[8,9]
T. brumale	Black musk truffle and winter truffle			European countries, especially France, Italy, Hungary, Serbia, Romania, and Slovenia	During winter–early spring	[10]
T. indicum	Chinese truffle	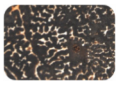		China and other Asian countries	November–March	[8,9]
White truffles						
T. magnatum	Piedmont white and white truffle			Native to Italian regions (Piedmont, Tuscany, and Emiglia Romagna)	Mid-October–end of December/end of January	[8,9]
T. borchii	Bianchetto and *T. albidum*			Europe, especially Italy, although rare in England, Switzerland, and Germany	During winter–early spring	[8,9]
T. oligospermum	Desert truffle	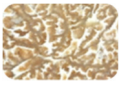		Mediterranean region and Morocco	October–May	[11]

All lower-value truffle species share morphological similarities with *T. melanosporum* or *T. magnatum*, which is why the distinction is not entirely trivial. This problem, combined with the price difference of truffles, makes truffles a product that is frequently affected by counterfeiting. Indeed, fraudulent practices have been detected in some products containing truffles [12]. In addition, truffle production is scarce and seasonal, which favors substitution or fraudulent practices and makes fresh truffles more vulnerable. However, truffle production is increasing year by year, especially in the orchards worldwide; e.g., *T. melanosporum* is cultivated in Spain, France, Italy, South Africa, Argentina, Chile, Australia, and New Zealand, among others [2].

Some analytical methods have been developed to detect possible fakes in truffle species, mainly based on genomics [13,14], proteomics [15], and aromatic profile studies [12]. However, these methods are time-consuming or only suitable for limited applications, e.g., the aroma changes during storage. Recently, further omics analyses (metabolomics and isotopolomics) using liquid chromatography–mass spectrometry (LC-MS) [16,17], near infrared spectroscopy (NIR) [18], as well as inductively coupled plasma mass spectrometry (ICP-MS) [19], were applied to detect differences between various truffle species.

In a previous study by us [16], a mass spectrometry-based non-targeted lipidomics approach was used to identify marker substances to distinguish the white truffle species *Tuber magnatum* and *Tuber borchii* and three black species, T. melanosporum, *T. indicum* and *T. aestivum*, with 100% accuracy. In the present study, this approach was further expanded, and a higher number of samples were used (188 vs. 78), as well as additional truffle species were investigated. Furthermore, the focus was on determining the geographical origin of the most valuable truffle species (*T. magnatum* and *T. melanosporum*).

2. Materials and Methods

2.1. Truffle Samples

In total, 188 truffle samples from the years 2017–2023 were measured. These included three white species: *T. borchii* (n = 10), *T. magnatum* (n = 25), *T. oligospermum* (n = 10); and five black species: *T. aestivum* (n = 29), *T. aestivum* var. *uncinatum* (n = 14), *T. brumale* (n = 17), *T. indicum* (n = 10), *T. melanosporum* (n = 73). For geographical studies, the two most valuable truffles (*T. magnatum* and *T. melanosporum*) were considered: The *T. magnatum* samples came from Bulgaria (n = 3), Croatia (n = 3), Italy (n = 12), and Serbia (n = 7). The *T. melanosporum* samples came from Argentina (n = 44), Spain (n = 20), Italy (n = 3), France (n = 3), and Australia (n = 3). Most of the samples were harvested directly from truffle orchards by the authors or supplied by an experienced truffle trader (La Bilancia, Trüffelhandels GmbH (Munich, Germany)).

Carpophores have been identified in the field based on the location and host plant, as well as their macroscopic features. Then, the truffles were transported to the laboratory in insulated boxes with cold packs and refrigerated at 4 °C until processing (between 3 and 12 h). This first classification was confirmed in the laboratory by microscopic identification according to the morphology of ascus and spores. Subsequently, the samples were brushed with a wet, soft brush, rinsed with ultrapure water, and forced air-dried in a laminar cabinet. Afterwards, the samples were frozen (−80 °C, 24 h) and stored in a freeze dryer (Cryodos-50 Telstar, Barcelona, Spain) to lyophilize them at −50 °C and at a vacuum of <10 mbar for 48 h. Then, the samples were ground and sieved to obtain a particle size of less than 0.5 mm and stored at −20 °C until further use.

2.2. Reagents

Acetonitrile, isopropanol, and methanol (all LC-MS grade), as well as chloroform (HPLC grade) and ammonium formate (≥95% puriss.), were purchased from Carl Roth GmbH (Karlsruhe, Germany). Water was obtained from a Merck Millipore water purification system (Direct-Q 3 UV-R system, Darmstadt, Germany). Hexakis(1*H*,1*H*,3*H*-perfluoropropoxy)phosphazene, purine, and LC/MS calibration standard for ESI-TOF were from Agilent Technologies (Santa Clara, CA, USA).

2.3. Truffle Metabolite Extraction

The extraction of the lipid fraction was carried out following a modified method from Bligh and Dyer [20]. For this purpose, 50 mg of the truffle powder was extracted with 750 µL of an ice-cold chloroform/methanol mixture (1:2, *v*/*v*) in a 2.0 mL reaction tube (Eppendorf, Hamburg, Germany). A cell disruption step using a ball mill (Omni International, Kennesaw, GA, USA) and two steel balls (3 mm in diameter, 1 min at 3 m s^{-1}) was carried out. Later, 250 µL chloroform and 500 µL water were added, and the samples were homogenized again with the ball mill (2 min at 3 m s^{-1}). The extracts were centrifuged at 16,000× *g* and 4 °C for 20 min (Sigma, Osterode, Germany). Afterwards, 100 µL of the lower phase (denser phase) from the centrifuged extract was diluted in 900 µL of eluent B of the chromatographic method. The solutions were centrifuged again (16,000× *g* and 4 °C for 10 min). From the supernatant obtained after centrifugation, 500 µL was transferred into a glass vial (Macherey-Nagel GmbH & Co. KG, Düren, Germany). To prevent changes in the analytes, the extraction process was carried out under ice cooling and with ice-cold solvents [16].

2.4. Liquid Chromatography and Mass Spectrometry Analysis

Liquid chromatography-mass spectrometry analyses were performed to detect possible marker compounds able to differentiate among truffle species and geographical origins. The measurements were carried out according to a method already developed for truffles [16]. For the analyses, an UHPLC system (1290 Infinity II, Agilent Technologies) coupled with an Agilent 6560 IM-QTOF-MS instrument (Agilent Technologies), equipped with an ESI source (Dual Jet Stream, Agilent Technologies) and a gas kit (Alternate Gas Kit, Agilent Technologies), was used. A reversed-phase C18 column (1.7 µm, 150 × 2.1 mm, Phenomenex, Aschaffenburg, Germany) with the temperature at 50 °C was applied during analysis. The gradient elution was carried out at a flow of 0.25 mL/min with water (A) and isopropanol/acetonitrile (3:1, *v*/*v*) (B). Both eluents contained 0.1 mmol/L ammonium formate. The gradient was performed as follows: 0–2 min, 55% (B), 2–4 min, 55–80% (B); 4–22 min, 80–100% (B); 22–23 min, 100% (B); 23–24 min, 100–55% (B); and 24–30 min, 55% (B). The ESI source was operated in the positive ionization mode with the following settings: gas temperature of 300 °C; drying gas flow rate of 12 L min^{-1}; nebulizer at 35 psi; sheath gas temperature of 275 °C; sheath gas flow rate of 12 L min^{-1}; capillary voltage of 3500 V; and nozzle voltage of 250 V [21]. Prior to the measurements, the MS was calibrated using the Agilent Technologies ESI tune mix. MS/MS fragment spectra were recorded at 10, 20, 40, and 60 eV to identify the most relevant marker compounds. For this purpose, the ion mobility measurement mode was switched to the QTOF mode. All other measurement conditions were retained. MS and MS/MS measurements were performed in the range of *m*/*z* 50–1700. For ion mobility data acquisition, the IM trapping funnel was operated with nitrogen as drift gas and a pressure of 3.95 Torr. The other settings were as follows: frame rate of 1 frame per s; IM transient rate of 19 IM transients/frame; max drift time of 50 ms; trap fill time of 3200 µs; trap release time of 250 µs; multiplexing pulse sequence length of 4 bits; drift tube entrance voltage of 1574 V; drift tube exit voltage of 224 V; rear funnel entrance voltage of 217.5 V; and the rear funnel exit voltage of 45 V [21]. For calibration of drift times, the Agilent Technologies ESI tune mix was infused regularly into the mass spectrometer with the same parameters for 1 min. In each case, 4 µL of the sample extracts were injected. The white and black truffle sample groups were measured directly one after the other, but in one batch, in order to be able to draw conclusions between the two datasets if necessary. However, two quality control (QC) samples were prepared, one for the white truffle samples and one for the black truffle samples, in order to be able to check during the subsequent data analysis whether normalization methods were used correctly. Aliquots of either all white or all black truffle samples were used to prepare the QC samples, which were regularly injected every 9 measurements. The individual white and black truffle samples were measured randomly in order to avoid possible bias.

2.5. Data Processing and Identification

The procedure described by Creydt and Fischer for data processing was followed [16]. Firstly, the IM-TOF data files were demultiplexed by the PNNL PreProcessor software (version 2020.03.23) [22,23]. The settings selected were as follows: demultiplexing checked; moving average smoothing checked; *m*/*z* not used; drift of 3; chromatography/infusion of 3; signal intensity lower threshold of 20 counts; spikes checked and removed; and saturation repair not checked. Later, the CCS calibration was performed by the IM-MS Browser software (version 10.0, Agilent Technologies, Santa Clara, CA, USA). Also, the Mass Profiler software (version 10.0, Agilent Technologies) was used for the four-dimensional feature finding (*m*/*z* ratios, retention times, CCS values, and signal intensities). The following parameters were selected: restrict RT to 0.0–23.0 min; ion intensity > 150.0 counts; isotope model as common organic (no halogens); limit charge states to a range of 1–2; report single-ion features with a charge state z = 1; RT tolerance = ±10.0% + 0.50 min; DT tolerance = ±1.5%; tolerance = ±20.0 ppm + 2.0 mDa; and Q-Score > 70.0. The parameters chosen were based on empirical values in order to obtain an appropriate bucket table. The incorrect assignment of isomers, which can sometimes occur, was reduced with the

instrument used due to the additional separation provided by ion mobility. The features obtained had to be detectable in at least 30% of all samples.

The received data tables were exported as xls files and then converted to csv format. Subsequently, MetaboAnalyst 5.0 software (http://www.metaboanalyst.ca, accessed on 20 May 2023) was used for further data analysis. Missing values were replaced with the smallest values with which a feature could still be detected. Also, sum normalization and autoscaling were performed. Afterwards, plots of principal component analysis (PCA) or partial least squares discriminant analysis (PLS-DA) were computed to estimate variances, sample distribution, and homologies between sample groups. The relevant marker substances were selected by carrying out a *t*-test (for two groups) or analysis of variance (ANOVA, for more than two groups) as well as using false discovery rates (FDRs) [24]. MS/MS spectra were recorded from the 100 most relevant marker compounds. The Lipid Annotator software (version 1.0, AgilentTechnologies, Santa Clara, CA, USA) as well as the two databases LipidMaps [25] and FooDB [26] were used to support compound identification. In addition, the tentative identification was checked with CCS values according to the LipidCCS database or LipidCCS Predictor and based on the retention times obtained using liquid chromatographic separation [27,28]. According to the metabolomics guidelines of Sumner et al., the identification measures performed correspond to level 2 [29].

3. Results

The two datasets (black and white truffle samples) were analyzed together with the QC samples for quality assessment and to identify potential outliers. The two PCA score plots (Figure S1) show that the measurements were reproducible, as the QC samples are almost superimposed in both cases. As seen in Figure S1A,B, it is clear that the QC samples are close to the center of the PCA, indicating that the pre-processing of the data was carried out in an appropriate manner. The slight deviation of the QC samples in Figure S1A may result from the imputation of the missing values or from the heterogeneity of the samples and is negligible. However, to ensure that there really are no deviations during the measurements, we checked the relative standard deviations of the peak areas of individual signals. These were less than 10%, so it can be concluded that no bias occurred during the measurements. The PCA score plot showed distinct separation for white truffle samples based on species, while black truffle samples displayed more overlap.

3.1. Data Analysis of the White Truffle Samples

The bucket table of the white truffle species samples contained 2729 features. Using ANOVA tests and the calculation of FDRs, 849 features were classified as significantly different (FDRs $\leq$ 0.05) in the three sample groups. The group distribution in the PCA score plot was clear, despite some slight overlays (Figure S1A). The outcome of a PLS-DA calculation along with the corresponding leave-one-out cross-validation (LOOCV) supported these results. The Q^2-value was 0.91 for two components, demonstrating a clear separation of the three sample groups, although some overlaps were evident in the PCA.

MS/MS fragment spectra were recorded from the 100 features with the smallest FDRs, and 40 signals belonging to different classes could be successfully identified. These categories included 2 ceramides (Cers), 15 glycerolipids, 5 diacylglyceryltrimethylhomoserines, and 15 phospholipids (Table 2). The fact that not all signals could be completely identified is a common challenge in metabolomics analyses, as entries in the relevant databases are currently often missing.

The metabolites were identified based on the adduct ions, the fragments generated, and the CCS values. Diacylglyceryl-O-4′-(*N*,*N*,*N*-trimethyl) homoserine (DGTS) derivatives could be detected as $[M+H]^+$-adducts and showed two characteristic fragments at m/z 144.10 ($C_7H_{14}NO_2^+$) and m/z 236.15 ($C_{10}H_{22}NO_5^+$) in positive ionization mode [30]. As far as we know, only Creydt and Fischer [16] reported CCS values for DGTS (36:3) (288.6 Å^2), which is very similar to the results in this study (289.4 Å^2).

Table 2. Identified key metabolites of the white truffle samples with their LC-IM-MS data, which show a dependency due to different white truffle species.

Tentative Compound	Proposed Formula	Adduct	RT (min)	*m*/*z* Experimental	*m*/*z* Theoretical	Error (ppm)	Relevant Fragments	CCS Value Measured [Å^2]	CCS Value Calculated [Å^2]	Delta CCS [%]	FDR
Ceramides											
Cer (34:0; O3)	C34H69NO4	$[M+H]^+$	9.909	556.5302	556.5312	2.28	538.52 (48); 520.51 (13); 284.29 (22); 20 eV	260.03	261.8	2.0	3.43×10^{-5}
Cer (38:5;O2)	C38H67NO3	$[M+H]^+$	10.095	586.5205	586.5199	0.90	324.28 (34); 306.28 (100); 20 eV	256.04	-	-	1.75×10^{-7}
Glycerolipids											
DG (33:4)	C36H62O5	$[M+H]^+$	6.532	575.4683	575.4671	0.17	557.45 (32); 379.33 (100); 20 eV	250.98	249.5–249.7	0.0	7.84×10^{-5}
DG (36:3)	C39H70O5	$[M + NH_4]^+$	11.704	636.5561	636.5564	0.40	601.52 (47); 339.29 (100); 20 eV	262.18	261.5–263.6	0.0	1.00×10^{-10}
DG (36:4)	C39H68O5	$[M+H]^+$	10.891	617.5139	617.5121	−3.00	599.50 (31); 339.29 (24); 20 eV	258.31	258.3−261.1	3.0	2.01×10^{-4}
DG (36:5)	C39H66O5	$[M + NH_4]^+$	9.831	632.5252	632.5252	0.57	337.27 (100); 10 eV	254.92	256.6–258.1	1.0	8.00×10^{-4}
DG (38:5)	C41H70O5	$[M+H]^+$	12.668	643.5279	643.5275	−3.27	339.29 (100); 40 eV	265.1	262.4–263.9	3.0	1.00×10^{-2}
TG (50:2)	C53H98O6	$[M + NH_4]^+$	19.412	848.7709	848.7700	−0.20	575.50 (100); 551.50 (37); 20 eV	315.74	310.3–314.1	0.0	9.85×10^{-4}
TG (51:3)	C54H98O6	$[M + NH_4]^+$	19.140	860.7711	860.7703	0.16	563.50 (100); 20 eV	316.13	311.4–315.2	0.0	1.15×10^{-2}
TG (52:5)	C55H96O6	$[M + NH_4]^+$	17.985	870.7550	870.7540	−0.37	599.50 (58); 573.49 (100); 20 eV	314.91	310.1–315.1	1.0	1.41×10^{-5}
TG (52:5).1	C55H96O6	$[M + NH_4]^+$	18.083	870.7555	870.7564	2.09	597.49 (72); 573.49 (100); 20 eV	315.37	310.7–315.1	2.0	1.16×10^{-3}
TG (54:4)	C57H102O6	$[M + NH_4]^+$	19.780	900.8019	900.8029	1.62	601.52 (100); 20 eV	324.17	319.3–323.8	2.0	5.24×10^{-3}
TG (55:4)	C58H104O6	$[M + NH_4]^+$	19.626	914.8177	914.8165	−0.69	617.55 (100); 20 eV	326.65	322.7–325.0	1.0	8.70×10^{-13}
TG (55:5)	C58H102O6	$[M + NH_4]^+$	19.201	912.8021	912.8011	−0.41	615.53 (100); 601.52 (48); 20 eV	324.93	321.1–323.3	0.0	8.05×10^{-16}
TG (57:7)	C60H106O6	$[M + Na]^+$	14.426	945.7879	945.7879	−2.82	805.55 (35); 10 eV	329.73	326.2–330.9	3.0	2.71×10^{-5}
TG (61:5)	C64H110O6	$[M+H-H_2O]^+$	17.245	957.8234	957.8275	−4.28	/	333.91	337.3–337.5	-	1.34×10^{-11}
TG (61:6)	C64H112O6	$[M+H-H_2O]^+$	17.565	959.8401	959.8432	−3.15	/	336.07	338.3–339.2	-	4.55×10^{-12}
DGTS (36:1)	C46H87NO7	$[M+H]^+$	12.053	766.6560	766.6554	−0.17	502.41 (66); 236.15 (100); 40 eV	308.71	-	-	3.40×10^{-3}
DGTS (36:3)	C46H83NO7	$[M+H]^+$	10.017	762.6243	762.6243	−1.75	500.39 (8); 236.15 (7); 20 eV	289.36	-	-	8.80×10^{-4}
DGTS (38:1)	C48H91NO7	$[M+H]^+$	13.290	794.6862	794.6862	−0.79	236.15; (100); 40 eV	299.50	-	-	1.77×10^{-16}
DGTS (38:2)	C48H89NO7	$[M+H]^+$	12.106	792.6713	792.6704	−0.99	500.40 (26); 236.14 (100); 144.10 (16); 40 eV	298.38	-	-	1.77×10^{-16}
DGTS (45:2)	C55H103NO7	$[M+H]^+$	16.183	890.7813	890.7808	0.08	617.51 (100); 575.50 (34); 20 eV	320.88	-	-	4.08×10^{-21}

Table 2. *Cont.*

Tentative Compound	Proposed Formula	Adduct	RT (min)	*m*/*z* Experimental	*m*/*z* Theoretical	Error (ppm)	Relevant Fragments	CCS Value Measured [Å^2]	CCS Value Calculated [Å^2]	Delta CCS [%]	FDR
Phospholipids											
LPC (16:0)	C24H50NO7P	$[M+H]^+$	6.421	496.3407	496.3406	2	184.07 (96); 104.10 (100); 20 eV	229.99	232.3–233.0	2.0	1.03×10^{-22}
LPC (18:1)	C26H52NO7P	$[M+H]^+$	6.012	522.3561	520.3555	0.16	184.07 (100); 20 eV	234.36	229.7	-	2.94×10^{-4}
LPC (18:2)	C26H50NO7P	$[M+H]^+$	6.210	520.3397	520.3410	2.38	184.07 (100); 20 eV	226.92	233.6	2.0	3.29×10^{-6}
LPC (18:2).1	C26H50NO7P	$[M+H]^+$	6.549	520.3409	520.3403	1.03	184.07 (100); 20 eV	228.08	233.6	1.0	4.00×10^{-2}
PC (34:1)	C42H82NO8P	$[M+H]^+$	5.692	760.5825	760.5844	−0.90	184.07 (100); 20 eV	286.97	289.4–291.3	1.0	2.68×10^{-12}
PC (34:1).1	C42H82NO8P	$[M+H]^+$	6.557	760.5838	760.5817	−4.45	184.07 (100); 20 eV	287.32	289.4–291.3	4.0	1.18×10^{-2}
PC (34:2)	C42H80NO8P	$[M+H]^+$	5.313	758.5689	758.5693	−0.83	184.07 (100); 20 eV	284.92	285.8–288.8	0.0	5.09×10^{-7}
PC (36:2)	C44H84NO8P	$[M+H]^+$	11.211	786.6051	786.6004	0.42	184.07 (100); 20 eV	292.05	290.5–295.4	0.0	8.35×10^{-15}
PC (36:2).1	C44H84NO8P	$[M+H]^+$	8.573	786.6195	786.6010	0.34	184.07 (100); 20 eV	297.02	290.5–295.4	0.0	1.07×10^{-4}
PC (36:4)	C44H80NO8P	$[M+H]^+$	16.623	782.5676	782.5685	0.47	184.07 (100); 20 eV	286.32	285.0–291.3	1.0	5.31×10^{-13}
PC (36:5)	C44H78NO8P	$[M+H]^+$	17.715	780.5526	780.5526	−1.52	184.07 (100); 20 eV	287.91	285.2–289.1	2.0	5.75×10^{-3}
PC (38:3)	C46H86NO8P	$[M+H]^+$	9.723	812.6178	812.6178	1.75	184.07 (100); 20 eV	295.74	294.6–297.4	2.0	4.60×10^{-3}
PE (34:1)	C39H76NO8P	$[M+H]^+$	11.875	718.5379	718.5474	−1.58	577.52 (100); 20 eV	275.70	276.1–280.4	0.0	6.91×10^{-3}
PE (36:4)	C41H74NO8P	$[M+H]^+$	9.908	740.5225	740.5225	0.03	599.50 (100); 20 eV	274.34	275.0–280.2	0.0	2.57×10^{-7}
PE (38:4)	C43H78NO8P	$[M+H]^+$	10.845	768.5541	768.5533	−0.63	627.53 (100); 599.50 (21); 20 eV	281.76	279.4–286.9	1.0	1.67×10^{-16}

The LipidCCS database and LipidCCS Predictor were used for CCS database values. The numbers in brackets represent the relative intensity of the fragments, based on the highest signal in the MS/MS spectrum.

Phospholipids, and in particular phosphatidylcholines (PCs), were also suitable for species differentiation. PCs were identified by $[M+H]^+$-adducts and the fragment m/z 184.07 ($C_5H_{15}NO_4P^+$) in the MS/MS spectra. This fragment is due to the loss of head group [31]. The compound lysophosphatidylcholine (LPC) (18:2) was identified two times, but at different retention times (RTs) (6.0 and 6.5 min) and with different CCS-values (234.4 $Å^2$ and 228.1 $Å^2$, respectively), so they might be isomers. For this reason, these isomers were labelled with "1" after the name, i.e., LPC (18:2), LPC (18:2).1. All the phosphatidylethanolamine (PEs) compounds listed in Tables 2 and 3 showed fragments resulting from the neutral loss of the polar head group (m/z 141); e.g., PE (34:1) with m/z 718.5 showed a fragment of m/z 577.5, being the difference of m/z 141 [31].

Both PCs, PEs, and DGTS are zwitterionic lipids that are mainly found in membranes and are assumed to complement each other in their functions or to serve as a substitute. While PCs and PEs are relatively widespread in the plant kingdom, DGTS derivatives have so far mainly been detected in lower organisms such as algae or fungi. Due to the mutual relationships between these substance classes, it is understandable that compounds of these substance classes are conspicuous as marker compounds [32–34].

Cers also showed potential as marker substances and could be detected as $[M+H]^+$-adducts. Their identification by MS/MS spectra was mainly based on the neutral loss of two water molecules [35]. The identification of Cer (34:0; O3) could be confirmed based on the CCS value (LipidCCS database). However, to our knowledge, CCS values for Cer (38:5; O2) have not yet been published. Nevertheless, it is also possible to calculate CCS values with the help of algorithms if the exact structure, i.e., the position of the double bond, is known [36–38]. Unfortunately, it was not possible to fully elucidate the structure using the MS or MS/MS data, which is why we did not use this approach. Cers are involved in various signal transduction pathways, and they have been described previously in fungal material [39]. Due to their diverse functions, it is not surprising that the concentration of different Cers varies in the various truffle species.

The LipidCCS database and LipidCCS Predictor were used for database CCS values. The numbers in brackets represent the relative intensity of the fragments, based on the highest signal in the MS/MS spectrum. In addition, numerous diglycerides (DGs) and triglycerides (TGs) were conspicuous for distinguishing the truffle species. DG and TG compounds are characterized by the loss of the acyl side chains in MS/MS spectra [16,40]. The data obtained for the CCS values were confirmed by the LipidCCS database. DGs have a physiological role in distinct cellular compartments and metabolic pathways, whereas TGs function primarily as storage molecules for fatty acyl chains [40,41].

The resulting PCA score plot based on these identified marker compounds is shown in Figure 1A. The plot revealed a clear clustering among truffle species. The Q^2-value of the LOOCV was 0.83 for two components, indicating excellent separation of the three sample groups. Figure 1B highlights some of the most suitable marker compounds as examples. For instance, using Cer (34:0; O3), it was possible to distinguish *T. borchii* from the rest of the white truffle species. In the case of DG (36:5), the highest concentration could be detected in the *T. magnatum* truffles. Therefore, by means of DG (36:5), it was possible to almost distinguish the *T. magnatum* samples from the other truffle species. In addition, using PC (36:2).1 and TG (50:2), *T. oligospermum* truffles could be distinguished from the *T. magnatum* and *T. borchii* samples. In summary, only with these four markers could the white truffle species be differentiated from each other.

Table 3. Identified key metabolites of the black truffle samples with their LC-IM-MS data, which show a dependency due to different black truffle species.

Tentative Compound	Proposed Formula	Adduct	RT (min)	*m*/*z* Experimental	*m*/*z* Theoretical	Error (ppm)	Relevant Fragments	CCS Value Measured [Å^2]	CCS Value Calculated [Å^2]	Delta CCS [%]	FDR
Ceramides											
Cer (34:1; O2)	C34H67NO3	$[M+H]^+$	10.198	538.5206	538.6164	2.29	264.27 (100); 20 eV	254.03	255.5	2.0	8.32×10^{-5}
Cer (34:2; O2)	C34H65NO3	$[M+H]^+$	9.611	536.5050	536.5050	2.39	518.50 (9); 282.28 (23); 264.27 (100); 20 eV	255.30	250.2	2.0	3.93×10^{-5}
Cer (34:0; O2)	C34H69NO3	$[M+H]^+$	10.629	540.5363	540.5479	2.37	/	259.76	260.2	2.0	1.00×10^{-2}
Cer (36:4; O2)	C36H65NO3	$[M+H]^+$	10.191	560.5027	560.5052	−1.83	264.27 (100); 40 eV	249.95	-	-	5.90×10^{-1}
Cer (36:6; O2)	C36H61NO3	$[M+H]^+$	9.563	556.5298	556.4720	−0.76	264.27 (22); 20 eV	257.32	261.8	0.0	7.97×10^{-21}
Cer (42:0; O4)	C42H85NO5	$[M+H]^+$	13.840	684.6497	684.6505	−0.51	264.27 (21); 20 eV	285.74	287.4	-	1.60×10^{-4}
HexCer (37:3; O2)	C43H79NO8	$[M+H]^+$	9.504	738.5885	738.5885	0.89	599.50 (31); 40 eV	284.54	-	-	1.12×10^{-3}
Glycerolipids											
DG (36:3)	C39H70O5	$[M + NH_4]^+$	11.595	636.5567	636.5567	0.89	339.29 (100); 20 eV	261.26	261.2–263.6	1.0	4.48×10^{-2}
DG (36:3).1	C39H70O5	$[M + Na]^+$	11.606	641.5119	641.5117	0.57	337.37 (100); 40 eV	263.34	261.3–263.7	1.0	4.96×10^{-3}
DG (41:3)	C44H80O5	$[M + NH_4]^+$	13.844	706.6319	706.6322	−3.63	684.65 (100); 60 eV	284.77	287.7	4.0	2.85×10^{-7}
TG (48:2)	C51H94O6	$[M + NH_4]^+$	18.381	820.7400	820.7394	1.41	575.50 (73); 20 eV	307.84	305.5–309.2	1.0	1.90×10^{-10}
TG (50:2)	C53H98O6	$[M + NH_4]^+$	19.153	848.7700	848.7700	−0.2	603.53 (12); 575.50 (100); 20 eV	314.51	310.3–314.1	0.0	1.84×10^{-1}
TG (50:3)	C53H96O6	$[M + NH_4]^+$	18.432	846.7543	846.7543	−0.26	601.52 (43); 575.50 (65); 20 ev	308.93	307.7–312.1	0.0	4.54×10^{-4}
TG (50:3). 1	C53H96O6	$[M + Na]^+$	18.416	851.7104	851.7092	−0.86	/	311.07	307.7–312.0	1.0	3.30×10^{-5}
TG (50:4)	C53H94O6	$[M + NH_4]^+$	17.712	844.7399	844.7460	1.25	599.50 (22); 573.49 (20); 20 eV	309.44	305.6–310.2	1.0	4.46×10^{-12}
TG (52:1)	C55H104O6	$[M + NH_4]^+$	20.531	878.8173	878.8185	0.21	605.55 (92); 577.52 (100); 40 eV	323.00	316.2–321.9	0.0	1.73×10^{-5}
TG (52:2)	C55H102O6	$[M + NH_4]^+$	20.273	876.8034	876.8042	2.25	603.54 (45); 577.52 (100); 40 eV	321.31	314.9–320.7	2.0	7.87×10^{-4}
TG (52:2). 1	C55H102O6	$[M + Na]^+$	19.823	881.7599	881.7513	3.54	/	320.35	314.9–320.7	3.0	2.99×10^{-3}
TG (52:3)	C55H100O6	$[M + Na]^+$	19.149	879.7424	879.7313	1.39	/	317.94	312.8–318.7	1.0	6.57×10^{-2}
TG (52:4)	C55H98O6	$[M + NH_4]^+$	18.514	872.7705	872.7709	0.39	575.50 (100); 20 eV	316.54	312.4–316.8	0.0	8.87×10^{-3}
TG (52:4). 1	C55H98O6	$[M + Na]^+$	18.475	877.7260	877.7260	0.51	597.48 (29); 40 eV	315.44	312.4–316.8	1.0	9.49×10^{-4}
TG (52:5)	C55H96O6	$[M + NH_4]^+$	17.747	870.7542	870.7542	−0.37	599.50 (41); 573.49 (100); 40 eV	313.88	310.7–315.1	0.0	7.80×10^{-4}
TG (52:6)	C55H94O6	$[M + NH_4]^+$	17.040	868.7392	869.5442	0.39	599.50 (56); 571.47 (100); 20 eV	311.58	309.1–313.7	0.0	2.03×10^{-5}

Table 3. *Cont.*

Tentative Compound	Proposed Formula	Adduct	RT (min)	*m*/*z* Experimental	*m*/*z* Theoretical	Error (ppm)	Relevant Fragments	CCS Value Measured [Å^2]	CCS Value Calculated [Å^2]	Delta CCS [%]	FDR
TG (53:4)	C56H100O6	$[M + NH_4]^+$	18.918	886.7863	886.7863	−0.56	/	319.27	316.2–318.2	1.0	2.87×10^{-6}
TG (54:1)	C57H108O6	$[M + NH_4]^+$	21.134	906.8485	906.8514	0.09	605.55 (100); 20 eV	328.93	321.7–327.3	0.0	2.61×10^{-4}
TG (54:3)	C57H104O6	$[M + NH_4]^+$	20.288	902.8172	902.8177	0.09	603.53 (100); 20 eV	325.37	319.7–325.7	0.0	5.65×10^{-4}
TG (54:4)	C57H102O6	$[M + NH_4]^+$	19.662	900.8016	900.8016	0.15	601.52 (100); 20 eV	323.26	319.3–323.8	0.0	9.47×10^{-7}
TG (54:4). 1	C57H102O6	$[M + Na]^+$	19.359	905.7574	905.7547	0.61	625.52 (33); 603.54 (24); 40 eV	321.74	319.3–323.8	1.0	1.14×10^{-3}
TG (54:5)	C57H100O6	$[M + NH_4]^+$	19.014	898.7864	898.7849	0.66	601.52 (100); 40 eV	320.90	317.5–322.1	1.0	1.73×10^{-3}
TG (54:5). 1	C57H100O6	$[M + Na]^+$	18.895	903.7432	903.7432	2.74	623.50 (40); 40 eV	319.90	317.5–322–1	2.0	3.35×10^{-3}
TG (54:6)	C57H98O6	$[M + NH_4]^+$	17.877	896.7704	896.7122	0.27	599.50 (100); 40 eV	319.23	315.8–320.7	0.0	3.32×10^{-3}
TG (54:6; O2)	C57H98O8	$[M + NH_4]^+$	15.522	928.7610	928.7600	1.1	599.50 (40); 501.39 (100); 20 eV	321.15	–	-	1.14×10^{-2}
TG (56:1)	C59H112O6	$[M + NH_4]^+$	21.685	934.8806	934.8271	0.58	661.61 (45); 635.60 (100); 605.55 (26); 577.52 (68); 40 eV	334.41	327.0–331.3	1.0	1.52×10^{-4}
TG (56:2)	C59H110O6	$[M + NH_4]^+$	21.128	932.8646	932.8628	−1.38	659.60 (16); 633.58 (100); 603.54 (67); 575.50 (22); 40 eV	332.98	326.9–331.7	1.0	2.12×10^{-5}
TG (56:3)	C59H108O6	$[M + NH_4]^+$	20.554	930.8485	930.8485	0.09	601.52 (100); 20 eV	331.57	325.2–330.6	0.0	9.17×10^{-4}
TG (56:4)	C59H106O6	$[M + NH_4]^+$	19.985	928.8328	928.8319	−0.95	631.57 (100); 601.52 (37); 20 eV	329.34	323.9–329.0	0.0	6.50×10^{-9}
TG (56:5)	C59H104O6	$[M + NH_4]^+$	19.315	926.8172	926.8045	0.09	629.55 (100); 599.50 (43); 20 eV	327.78	322.6–327.4	0.0	1.16×10^{-4}
TG (56:6)	C59H102O6	$[M + NH_4]^+$	18.651	924.8019	924.7874	0.48	627.53 (100); 599.50 (60); 20 eV	325.73	320.9–325.9	0.0	4.24×10^{-12}
TG (57:2)	C60H112O6	$[M + NH_4]^+$	21.418	946.8809	946.8209	1.27	603.53 (69); 575.59 (59); 40 eV	335.12	329.7–332.9	1.0	3.98×10^{-3}
TG (58:1)	C61H116O6	$[M + NH_4]^+$	22.190	962.9112	962.9005	0.19	605.54 (92); 577.51 (100); 20 eV	340.04	332.0–336.0	0.0	1.52×10^{-4}
TG (58:2)	C61H114O6	$[M + NH_4]^+$	21.676	960.8956	960.8994	−1.24	603.45 (82); 575.50 (36); 20 eV	338.23	332.4–337.6	0.0	4.31×10^{-5}
TG (58:2). 1	C61H114O6	$[M + Na]^+$	21.650	965.8533	965.8444	2.69	/	336.37	332.4–337.6	3.0	3.35×10^{-3}
TG (58:3)	C61H112O6	$[M + NH_4]^+$	21.161	958.8801	958.8874	0.41	601.52 (100); 339.29 (3); 20 eV	336.23	331.4–337.5	0.0	1.12×10^{-7}
TG (58:4)	C61H110O6	$[M + NH_4]^+$	20.643	956.8648	956.8659	0.78	659.60 (100); 599.50 (83); 20 eV	333.74	330.4–336.0	1.0	6.86×10^{-6}
TG (59:3)	C62H114O6	$[M + NH_4]^+$	21.432	972.8966	972.8963	0.98	601.52 (100); 20 eV	338.45	335.1–338.2	1.0	1.72×10^{-4}
TG (58:6)	C61H106O6	$[M + Na]^+$	16.673	957.8245	957.7448	−0.05	/	332.44	322.44	0.0	6.5×10^{-2}
TG (60:2)	C63H118O6	$[M + NH_4]^+$	22.171	988.9273	988.9284	0.65	689.64 (53); 603.53 (100); 40 eV	343.68	337.6–343.2	1.0	1.56×10^{-4}
TG (60:4)	C63H114O6	$[M + NH_4]^+$	21.097	984.8957	984.8954	0.34	685.61 (72); 601.51 (100); 20 eV	340.28	336.7–342.9	0.0	2.21×10^{-3}

Table 3. *Cont.*

Tentative Compound	Proposed Formula	Adduct	RT (min)	*m*/*z* Experimental	*m*/*z* Theoretical	Error (ppm)	Relevant Fragments	CCS Value Measured [Å^2]	CCS Value Calculated [Å^2]	Delta CCS [%]	FDR
Diacylglyceryltrimethylhomoserines											
DGTS (34:1)	C44H83NO7	$[M+H]^+$	10.722	738.6238	738.5028	−0.58	599.50 (14); 236.15 (20); 40 eV	286.20	-	-	5.97×10^{-5}
DGTS (36:2)	C46H85NO7	$[M+H]^+$	10.962	764.6384	764.5200	−1.94	236.15 (43); 40 eV	291.47	-	-	5.58×10^{-17}
DGTS (36:3)	C46H83NO7	$[M+H]^+$	9.939	762.6243	762.6115	0.09	236.15 (100); 40 eV	288.28	-	-	8.83×10^{-12}
DGTS (36:4)	C46H81NO7	$[M+H]^+$	9.190	760.6065	760.6065	−2.74	498.38 (79); 236.15 (100); 40 eV	285.51	-	-	4.90×10^{-9}
LGDTS (18:2)	C28H51NO6	$[M+H]^+$	4.608	498.3802	498.3791	0.37	236.15 (100); 144.10 (8); 20 eV	224.29	-	-	4.92×10^{-3}
Phospholipids											
LPC (18:2)	C26H50NO7P	$[M+H]^+$	4.818	520.3401	520.3626	0.64	184.07 (100); 20 eV	227.86	233.6	1.0	5.60×10^{-4}
PC (36:4)	C44H80NO8P	$[M+H]^+$	12.913	782.5690	782.5677	−0.55	184.07 (100); 20 eV	285.96	284.7−288.6	1.0	3.30×10^{-15}
PE (34:2)	C39H74NO8P	$[M+H]^+$	10.302	716.5223	716.5223	−0.25	575.50 (100; 20 eV	272.70	273.0−277.5	0.0	1.34×10^{-5}
PE (36:2)	C41H78NO8P	$[M+H]^+$	11.583	744.5556	744.5256	2.45	603.54 (100); 20 eV	279.11	277.7−285.1	2.0	2.51×10^{-8}
PE (36:4)	C41H74NO8P	$[M+H]^+$	9.538	740.5224	740.5224	−0.11	599.50 (100); 20 eV	273.44	275.0−275.3	0.0	2.85×10^{-7}

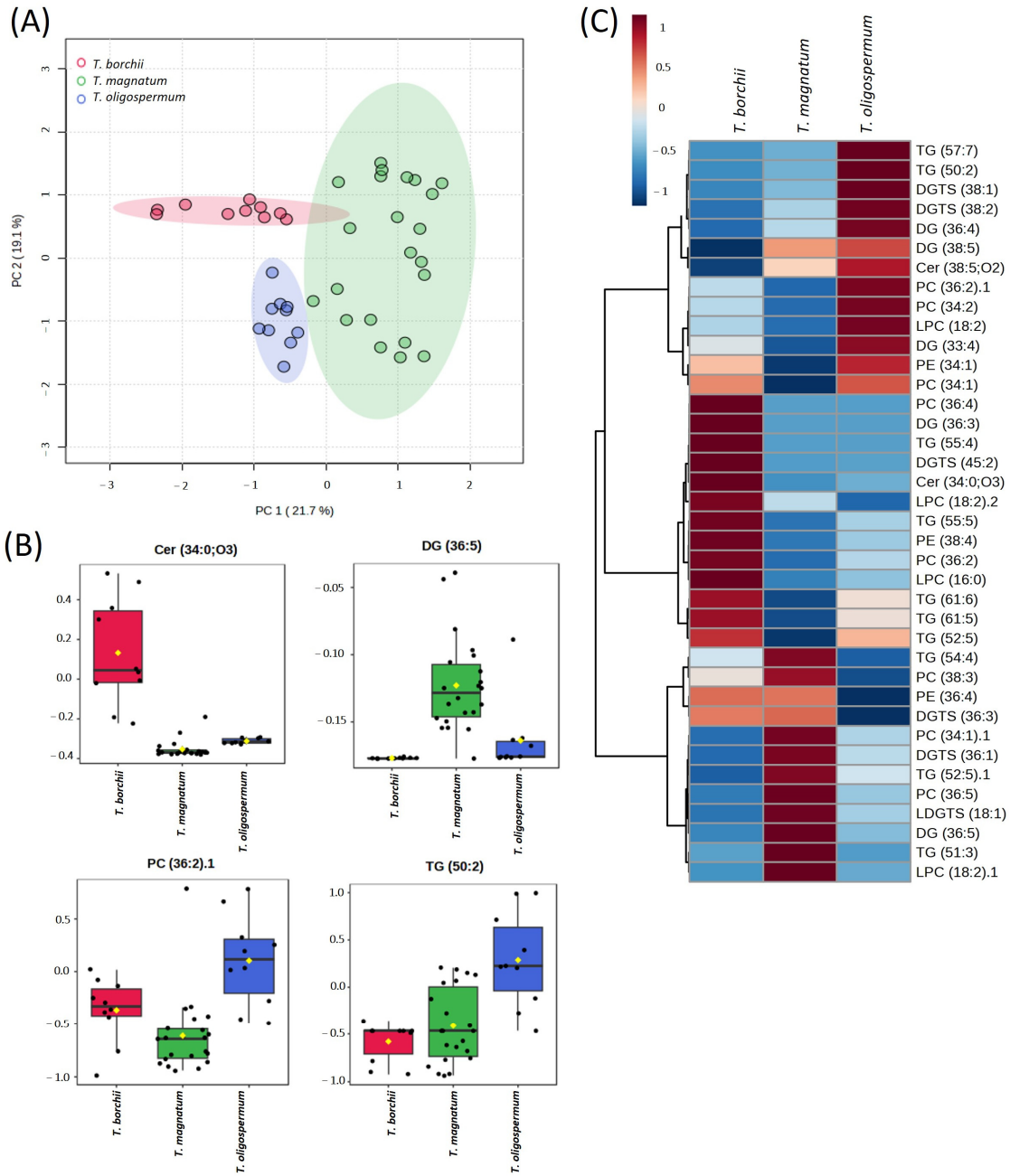

Figure 1. White truffle samples: (**A**) PCA score plot with all features detected; (**B**) selected marker compounds from white truffles; and (**C**) heatmap of metabolite profile (marker compounds selected) for each white truffle species.

The heatmap in Figure 1C indicates the correlation within the identified marker compounds. The profiles of the different truffle species varied. The *T. borchii* and *T. magnatum* samples showed similarities in three correlated metabolites: PC (38:3), PE (36:4), and DGTS (36:3). The *T. borchii* and *T. oliospermum* samples showed similarities in five correlated metabolites: PE (34:1), PC (34:1), TG (61:6), TG (61:5), and TG (52:5), these last three being correlated with each other. Only two metabolites, DG (38:5) and Cer (38:5; O2), showed comparable values regarding the profiles of the *T. magnatum* and the *T. oliospermum* samples.

In the previous study on which this study is based, 33 marker compounds were identified for the differentiation of *T. magnatum* and *T. borchii* truffles [16]. Some of them proved to be particularly suitable for differentiation in this study, which was to be expected.

An overview of these marker compounds together with a comparison of the identification parameters can be found in Table S1. In this context, the following compounds were noticeable: DGTS (36:3), DG (36:3), TG (50:2), PC (34:1), PC (34:1).1, and PC (34:2). As expected, the ratios of these compounds in this and the previous study were similar in relation to the *T. magnatum* and *T. borchii* samples. The *T. oligospermum* samples were not available in the first study [16], which is why no comparison could be made in this regard.

3.2. Data Analysis of the Black Truffle Samples

Following the white truffle analysis (Section 3.1), the same steps were applied to black truffle samples. The table of non-targeted measurements of the black truffle species included 479 features. After employing an ANOVA test to identify differences among the sample groups, the number of relevant features was reduced to 123 that showed significant variability between the groups. With this number of features, the samples were classified as significantly different in the five sample groups. Nevertheless, when comparing this dataset with the dataset of the white truffle species samples, the group distribution in the PCA score plot was less clear (Figure S1B). Some differences among groups could be found, but the 95% confidence regions overlap significantly. In the PLS-DA analysis, the Q^2-value of the LOOCV for the fifth component was 0.76, indicating significant differences.

To gain a better understanding of the relationships between the sample groups, a simpler evaluation was performed to compare the truffle species. When *T. melanosporum* truffles were compared with the rest of the species, the results obtained were similar: vs. *T. aestivum* (0.77 for fifth components), vs. *T. brumale* (0.71 for fourth components), vs. *T. indicum* (0.57 for third components), vs. *T. uncinatum* (0.74 for third components). These Q^2-values indicate that the model proved to be predictable, despite the data being complex. This is underscored by the fact that the PCA explained 29.9% of the variance with just the first two components.

Following the same method as for the white truffle samples, the MS/MS fragment spectra of the most significant 100 features (smallest FDRs) were recorded. Out of these, a total of 57 features were identified (Table 3). Among these were 7 Cers, 40 glycerolipids, 5 diacylglyceryltrimethylhomoserine derivatives, and 5 phospholipids.

In this case, the number of TGs was more than double compared to the compounds identified in the white truffle species. TGs, composed of glycerol and three fatty acids, have an important role as transporters of fatty acids and serve as an energy source (see Section 3.1). Some of the fatty acids are associated with key aromatic compounds in truffles. For example, linolenic acid is transformed into 1-octen-3ol, 3-octanol, or 3-octanone because of the 10-lipoxygenase enzyme. It can also be converted to hexanal and hexanol by the 13-lypoxygenase and alcohol dehydrogenase (ADH) enzymes. Moreover, the compound α-linolenic acid is converted into 3-hexenal and then 2-hexenol or 2-hexenal via the 3-lypoxygenase pathway [42,43].

As observed with the white truffles and in the previous studies, some ceramides were again noticeable. Furthermore, different Cers (C_{18}-phytosphingosine or 4-sphingenine) and sphingolipid compounds were previously reported in *T. indicum* truffles [44,45]. Given their function (see Section 3.1), it was not surprising that the ceramides also contributed to the differentiation of the samples in this sample set. The same applies to the detected molecules from the substance classes DGTS, PC, and PE.

The PCA scores plot obtained using only the identified marker compounds is shown in Figure 2A. The five groups were clustered, but the resulting groups were overlaid. When performing a PLS-DA analysis, the Q^2-value of the LOOCV showed a value below 0.4 for five components. This value indicates that there are few differences between the five groups, and the model cannot separate the groups. When the different black truffle species were compared with each other, only these combinations resulted in a Q^2-value ≥ 0.5, which indicates larger differences between the sample groups: *T. aestivum* vs. *T. brumale* (0.53 for three components), *T. indicum* vs. *T. uncinatum* (0.65 for four components), *T. brumale* vs. *T. uncinatum* (0.58 for four components), *T. melanosporum* vs. *T. brumale* (0.53 for five

components), and *T. melanosporum* vs. *T. indicum* (0.57 for five components). These values indicate that the data correlation was quite difficult. This might be due to the number of *T. melanosporum* truffle samples, their different origins (Spain, France, Italy, Australia, and Argentina), or the range of harvest years (from 2017 to 2023). In addition, *T. aestivum* and *T. uncinatum* were grouped together and compared with the rest of the species. However, all the Q^2-values were lower when the species were compared separately. This approach was considered because *T. uncinatum* is described as an ecotype of the *T. aestivum* species. Therefore, the differences between these groups may not be so clear. Most often they are considered as the same species that were harvested at a different time.

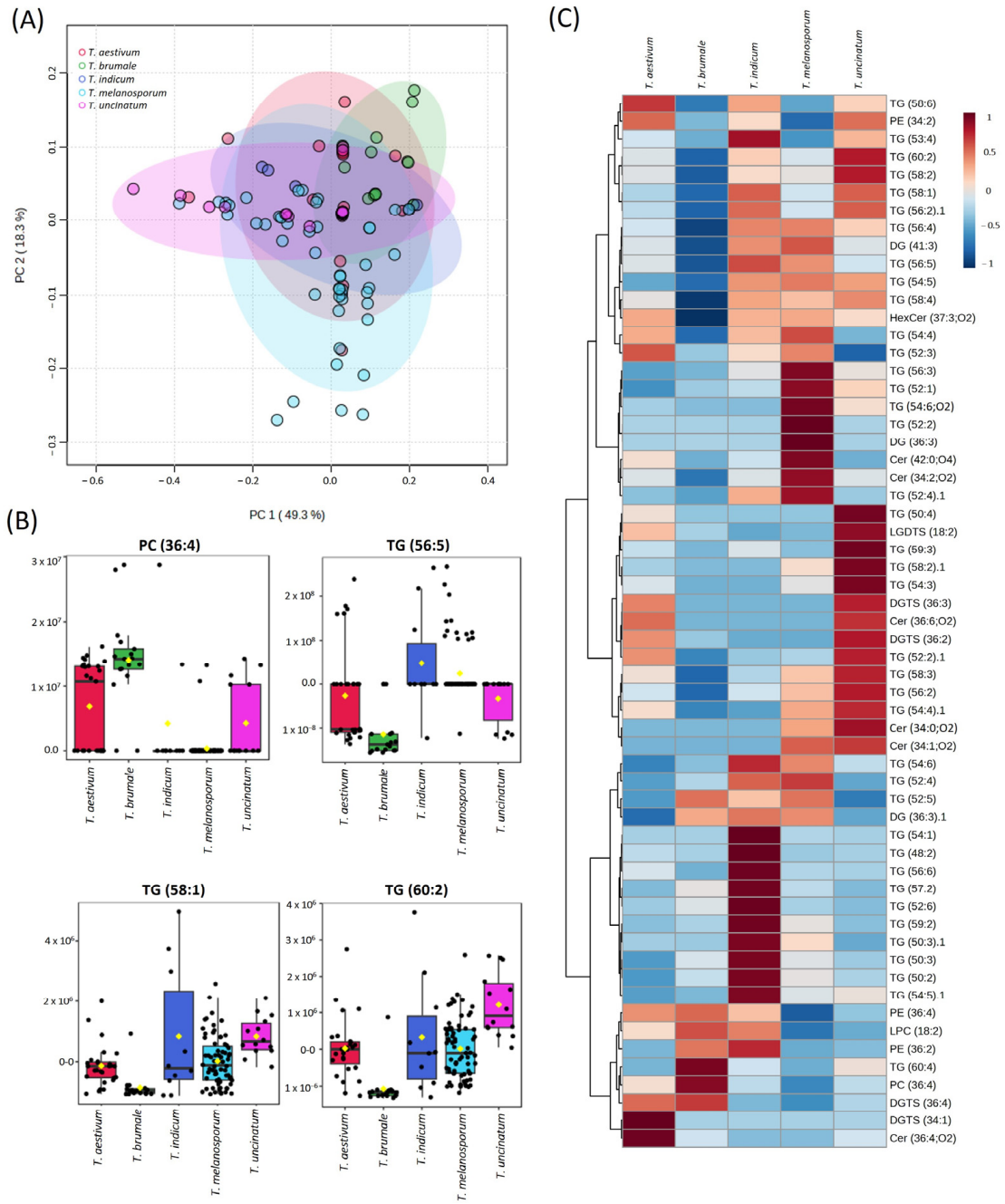

Figure 2. Black truffle samples: (**A**) PCA score plot with all features detected; (**B**) selected marker compounds from black truffles; and (**C**) heatmap of metabolite profile (marker compounds selected) for each black truffle species.

The black truffle species could be separated from each other on the basis of compounds such as PC (36:4), TG (56:5), TG 58:1, and TG (60:2) (Figure 2B). Furthermore, a heatmap was used to explore possible correlations between the identified metabolites (Figure 2C). *T. aestivum* and *T. uncinatum* showed the highest similarities in TG (58:6), PE (34:2), DGTS (36:3), Cer (36:6; O2), DGTS (36:2), TG (52:2).1, TG (52:3), TG (54:4), and HexCer (37:3; O2). However, *T. brumale* only shared DG (36:3).1 and TG (52:5) with *T. melanosporum* and *T. indicum*. These last two species showed a similar profile, since several DG and TG compounds were in both metabolomic profiles. When *T. melanosporum* and *T. aestivum* profiles were compared, only a few metabolites were correlated: HexCer (37:3; O2) (also positively correlated with *T. indicum* and *T. uncinatum*) and two glycolipids (TG (54:4) and TG (52:3)) also correlated with *T. indicum*. The heatmap revealed two distinct metabolomic profiles: one grouping *T. aestivum* and *T. uncinatum* together and the other comprising the remaining three truffle species.

Upon comparison with the results from the previous study, the marker compounds identified in this analysis were found to overlap with some of those previously noted (Table S1). This affected some of the Cers and the DGTS marker compounds. The relative intensity ratios between the sample groups were again quite similar. The DGTS markers were primarily detected with higher signal intensities in the *T. aestivum* and the ceramides in the *T. melanosporum* and *T. indicum* samples.

3.3. Identification of Marker Compounds for Distinguishing the Geographical Origin of T. magnatum and T. melanosporum Truffles

The geographical differentiation of the *T. magnatum* and *T. melanosporum* samples was carried out considering the previously described markers (Tables 2 and 3). The PCA score plots showed overlays in all groups (Figure S2A,B), and the Q^2-values were negative for two components for both *T. magnatum* and *T. melanosporum* locations. The negative and low Q^2-values results were to be expected since some of the sample groups were comparatively small. However, when only *T. magnatum* samples from Italy and Serbia were compared, the Q^2-value for two components was 0.8. To increase the Q^2-value, a selection of a few marker compounds was made. Only those features were considered that showed statistical differences when comparing samples with different geographic origins in the ANOVA test and that had already been identified in Sections 3.1 and 3.2, respectively.

The investigation of the geographical origin of the *T. magnatum* samples included the following compounds: PE (34:1), PC (34:1), LPC (18:2), TG (54:4), and TG (51:3). However, no clear clusters could be achieved in the PCA scores plot obtained, and the Q^2-value was negative (Figure S2C). These results indicated that the model was not predictive or was overfitted. Consequently, the LC-MS method approach to evaluate the geographical origin of *T. magnatum* did not work for this dataset. However, a metabolite profile with correlations is indicated in a heatmap (Figure 3A). Italy and Serbia locations showed a similar profile, especially with regard to two metabolite clusters: the combination of Cer (38:5; O2), DGTS (45:2), and LDGTS (18:1), as well as the combination of TG (52:5), PC (36:4), LPC (16:0), and TG (61:5). Despite the distance between these two countries, these similarities could be due to comparable soil or climate conditions, among other reasons. Bulgaria and Croatia, however, showed only one common metabolite (DG (38:5)), as well as with Italy (DGTS (42:2)). A higher number of samples might be necessary to obtain a more predictable model. The current norm that explains the truffle quality and indicates the truffle species that can be commercialized [46] does not contemplate the origin country of truffle species. Especially, *T. magnatum* from Italy is known worldwide and has even created a local quality brand. Hence, the existence of a robust method to detect *T. magnatum* among the neighboring countries might ensure the provenance of this truffle species.

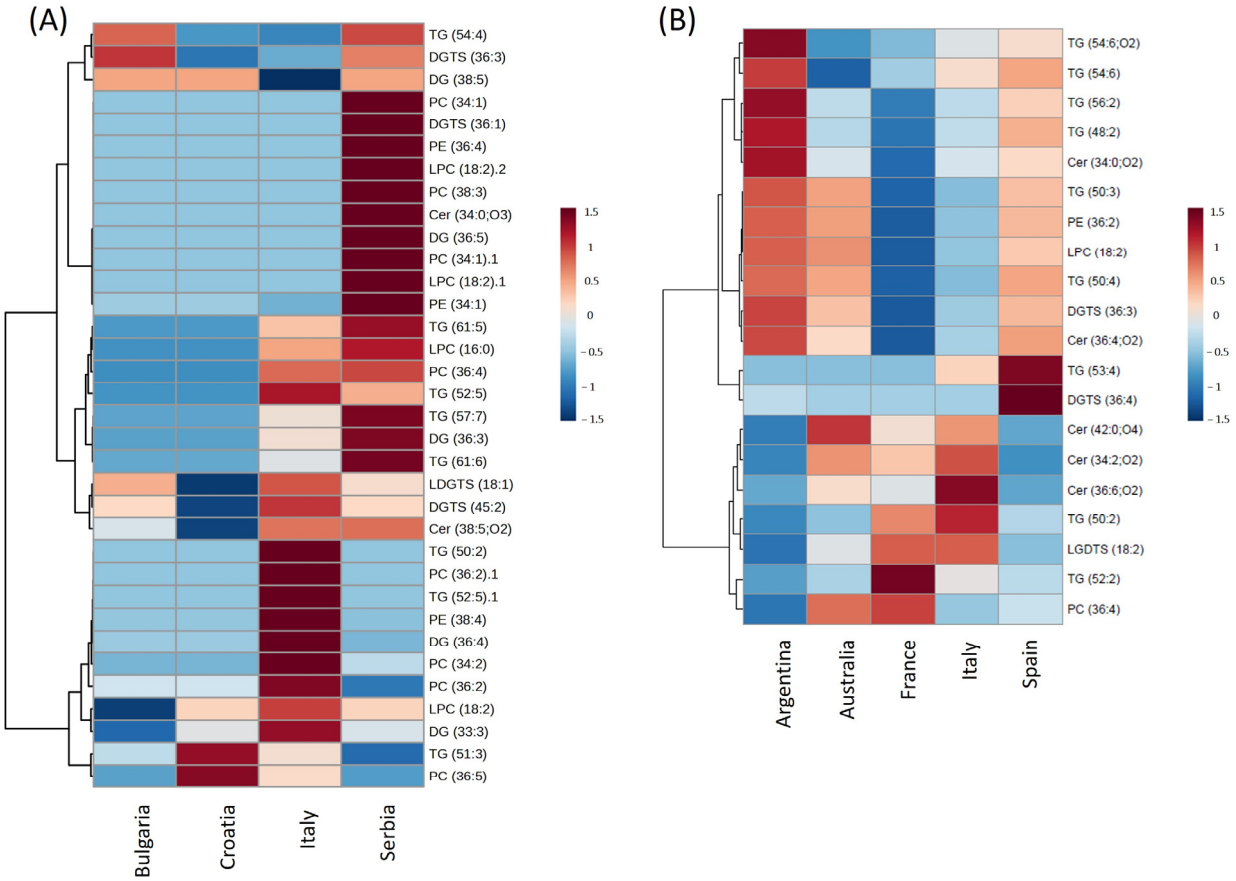

Figure 3. Heatmap of metabolite profile for (**A**) *Tuber magnatum* and (**B**) *Tuber melanosporum* sample locations.

In the *T. melanosporum* samples, which mostly originated from Argentina and Spain, as well as from Australia, France, and Italy, a very good separation could be seen in the PCA scores plot, even if some sample groups consisted of only a few individuals (Figure 4A). Spanish truffle samples were clearly different from the rest of the European samples (France and Italy). Also, samples from Australia and Argentina were separated from the Spanish samples. It was expected to obtain clearer differences between truffles from the northern and southern hemispheres, but the PCA did not show these disparities. The result of a PLS-DA calculation and the associated LOOCV was correspondingly good. The Q^2-value was 0.74 for two components and 0.81 for five components, indicating a good separation of the five sample groups.

The 20 following metabolites were selected to differentiate the geographical origins of the *T. melanosporum* samples: Cer (34:2; O2), Cer (34:0; O2), Cer (36:4; O2), Cer (36:6; O2), Cer (42:0; O4), TG (48:2), TG (50:2), TG (50:3), TG (50:4), TG (52:2), TG (53:4), TG (54:6), TG (54:6; O2), TG (56:2), LGDTS (18:2), DGTS (36:4), DGTS (36:6), LPC (18:2), PC (36:4), and PE (36:2). French truffles could be differentiated from the other locations by Cers (Cer (34:0; O2), Cer (36:4; O2)), whereas glycerolipids (TG (54:6), TG (54:6; O2), and TG 56:2) were useful for discriminating the Australian truffles (Figure 4B). Spanish and Argentinian truffles could be distinguished from the French or Italian truffles by Cer (36:4; O2), DGTS 36:3, and TG 48:2 metabolites. The markers Cer (34:2; O2), Cer (34:0; O2), Cer (36:4; O2), DGTS (36:6), TG (48:2), TG (54:6), TG (54:6; O2), and TG (56:2) were found to be useful to differentiate between *T. melanosporum* locations (Figure 3B). Moreover, the heatmap plot showed strong correlations between PC (36:4) and TG (52:2) or DGTS (36:4) and TG (53:4) to differentiate French and Spanish truffles, respectively. The metabolite Cer (36:6; O2) might be used to distinguish Italian fruiting bodies, whereas some triglycerides (TG (54:6),

TG (54:6; O2), TG (56:2), and TG (48:2)) could be used as potential markers for Argentinian truffles.

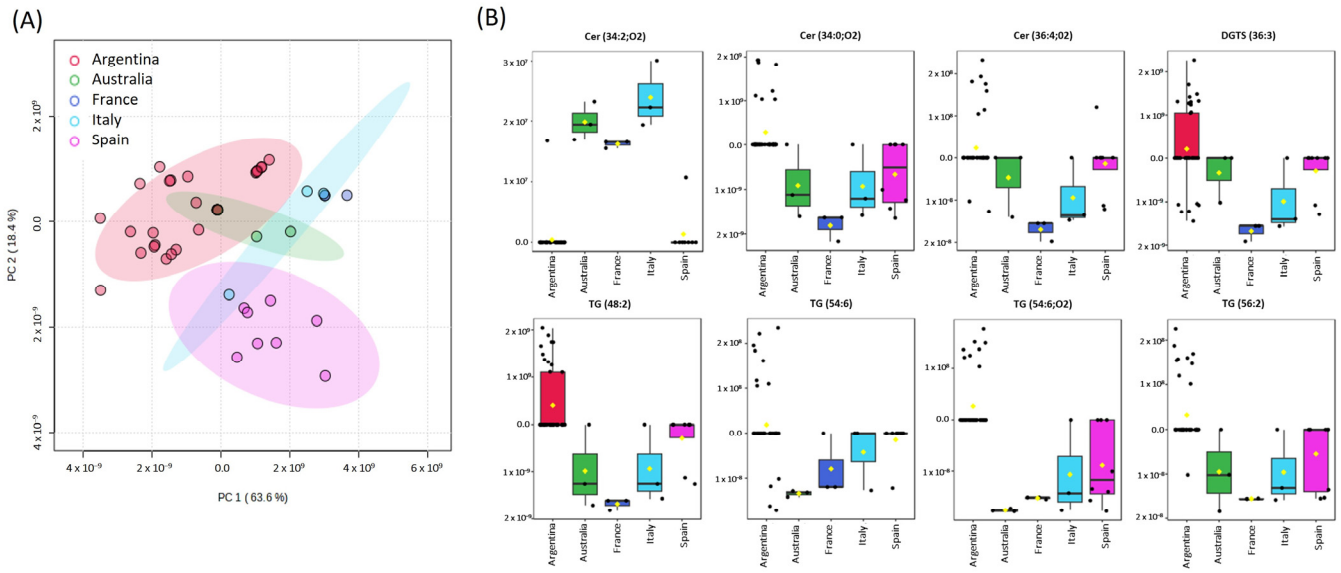

Figure 4. *T. melanosporum* truffle samples: (**A**) PCA score plot with selected features and (**B**) selected marker compounds from *T. melanosporum* geographical origin samples.

It could be observed that the profiles of truffles from Argentina and Spain exhibit clustering, while those from France and Italy were more similar. This might be due to the fact that Argentinian truffle trees, and probably Australian truffle trees as well, have been inoculated with Spanish *T. melanosporum* truffle spores. However, it could also be due to the different numbers of samples. Indeed, a recent study pointed out the similarity in the aromatic profile between Argentine and Spanish truffles in comparison with French or Italian ones [47]. The study of truffle volatile profiles has been widely studied for geographical origin determination [48–51]. Also, bioactive compounds such as sterols were studied in this regard [52]. Another study using an isotopolomic approach with ICP-MS was able to distinguish between the geographical origin of truffles with an accuracy of 75.0% (Italian and non-Italian samples) and 86.7% (Spanish and non-Spanish samples) [19]. In general, good clustering was obtained, showing that geographical origin influences the lipid profile of black truffles, despite some variables such as climate, soil, host tree, and post-harvest processing, among others. Based on these results, the LC-MS method presented in this study should be well suited for verifying the geographical origin of *T. melanosporum* truffles.

Today, there is neither a protected designation of origin (PDO) nor a protected geographical indication (PGI) for truffles. However, it is expected that some provinces in Spain, France, and Italy will introduce these indications. Therefore, this LC-MS method could be used to identify marker compounds for the quality control of possible PDO or PGI specifications.

4. Conclusions

The application of a lipidomics-based approach allowed the identification of three different white truffle species and five black truffle species. Using an LC-ESI-IM-QTOF-MS instrument, it was possible to detect up to 2000 features. Furthermore, based on the MS/MS fragment spectra and the CCS values, 37 and 57 markers, respectively, for distinguishing white and black truffle species could be identified. The most relevant key compounds included Cers, DGTS derivatives, phospholipids, and numerous glycerides. The method allowed us to clearly separate different locations of *T. melanosporum* truffles, but not the differentiation of various locations of *T. magnatum* samples. Further studies

in this direction regarding markers for substitution, freshness, and storage conditions are essential to support quality control in high-value products such as truffles. Research into these markers will help ensure product authenticity, detect possible adulteration, and assess freshness over time, addressing key quality attributes valued by consumers and the industry alike.

Supplementary Materials: The following supporting information can be downloaded at: https://www.mdpi.com/article/10.3390/agriculture14122350/s1. Figure S1: PCA scores plot of all measurements, including QC samples: (A) white truffle samples; (B) black truffle samples. Figure S2: (A) *T. magnatum* geographical origin samples PCA score plot with marker compounds; (B) *T. melanosporum* geographical origin samples PCA score plot with marker compounds; and (C) *T. magnatum* geographical origin samples PCA score plot with five marker compounds. Marker compounds from A and B are listed in Tables 2 and 3, respectively. Table S1: List of identified key metabolites in the present manuscript and their comparison with a previous study [16]) in white and black truffles.

Author Contributions: Conceptualization, E.T.-C. and M.C.; methodology, E.T.-C.; software, E.T.-C.; formal analysis, E.T.-C. and M.C.; investigation, E.T.-C.; resources, P.M. and M.F.; data curation, E.T.-C.; writing—original draft preparation, E.T.-C.; writing—review and editing, M.F. and M.C.; visualization, E.T.-C.; supervision, M.C.; funding acquisition, P.M. and M.F. All authors have read and agreed to the published version of the manuscript.

Funding: This research was supported by fellowship Ibercaja—CAI Estancias de Investigación number CM 11/22 as well as by Fondo Europeo Agrícola de Desarrollo Rural 2014–2022 (FEADER) in Aragón (Spain) (project "Organización, valorización y promoción de la Trufa Negra de Aragón"). The research leading to these results has received funding from the European Union under "Horizon 2020—the Framework Programme for Research and Innovation (2014–2020). Grant Agreement of the Project "Innovation in truffle cultivation, preservation, processing, and wild truffle resources management", INTACT, Project number 101007623". The project "Food Profiling—Development of analytical tools for the experimental verification of the origin and identity of food" (Funding reference number: 2816500914) is supported by means of the Federal Ministry of Food and Agriculture (BMEL) by a decision of the German Bundestag (parliament). Project support is provided by the Federal Institute for Agriculture and Food (BLE) within the scope of the program for promoting innovation. E.T.-C. has received the grant JDC2022-048252-I funded by MICIU/AEI/10.13039/501100011033 and "European Union NextGenerationEU/PRTR".

Data Availability Statement: The data presented in this study are available in this article.

Acknowledgments: This research was supported by Diputación Provincial de Zaragoza (DPZ) in Spain to provide some samples. The authors want to thank Trufas del Nuevo Mundo Company for providing some samples. Some of the samples were obtained through the "Food Profiling—Development of analytical tools for the experimental verification of the origin and identity of food". The graphical abstract was created in https://BioRender.com (accessed on 15 December 2024).

Conflicts of Interest: The authors declare no conflicts of interest.

References

1. Bonito, G.M.; Gryganskyi, A.P.; Trappe, J.M.; Vilgalys, R. A Global Meta-Analysis of Tuber ITS RDNA Sequences: Species Diversity, Host Associations and Long-Distance Dispersal. *Mol. Ecol.* **2010**, *19*, 4994–5008. [CrossRef] [PubMed]
2. Reyna, S.; Garcia-Barreda, S. Black Truffle Cultivation: A Global Reality. *For. Syst.* **2014**, *23*, 317–328. [CrossRef]
3. Costa, R.; Fanali, C.; Pennazza, G.; Tedone, L.; Dugo, L.; Santonico, M.; Sciarrone, D.; Cacciola, F.; Cucchiarini, L.; Dachà, M.; et al. Screening of Volatile Compounds Composition of White Truffle during Storage by GCxGC-(FID/MS) and Gas Sensor Array Analyses. *LWT—Food Sci. Technol.* **2015**, *60*, 905–913. [CrossRef]
4. Tejedor-Calvo, E.; García-Barreda, S.; Sánchez, S.; Morales, D.; Soler-Rivas, C.; Ruiz-Rodriguez, A.; Sanz, M.Á.; Garcia, A.P.; Morte, A.; Marco, P. Supercritical CO_2 Extraction Method of Aromatic Compounds from Truffles. *LWT* **2021**, *150*, 111954. [CrossRef]
5. Oliach, D.; Vidale, E.; Brenko, A.; Marois, O.; Andrighetto, N.; Stara, K.; Martínez de Aragón, J.; Colinas, C.; Bonet, J.A. Truffle Market Evolution: An Application of the Delphi Method. *Forests* **2021**, *12*, 1174. [CrossRef]
6. Benucci, G.M.N.; Csorbai, A.G.; Falini, L.B.; Marozzi, G.; Suriano, E.; Sitta, N.; Donnini, D. Taxonomy, Biology and Ecology of *Tuber Macrosporum* Vittad. and *Tuber Mesentericum* Vittad. In *True Truffle (Tuber spp.) in the World*; Springer: Cham, Switzerland, 2016; pp. 69–86.

7. Hall, I.R.; Stephenson, S.L.; Buchanan, P.K.; Yun, W.; Cole, A.L. *Edible and Poisonous Mushrooms of the World*; Timber Press: Portland, OR, USA, 2003; ISBN 0881925861.
8. Hall, I.; Brown, T.; Zambonelli, A. *Taming the Truffle*; Timber Press: Portland, OR, USA, 2007.
9. Luard, E. *Truffles*; Berry & Co., Ltd., Ed.; Frances Lincoln: London, UK, 2006.
10. Merényi, Z.; Varga, T.; Bratek, Z. *Tuber brumale*: A Controversial Tuber Species. In *Systematics and Biochemistry*; Springer: Cham, Switzerland, 2016; pp. 49–68.
11. Moreno-Arroyo, B.; Infante, F.; Pulido, E.; Gómez, J. The Biogeography and Taxonomy of *Tuber Oligospermum* (Tul. & C. Tul.) Trappe (*Ascomycota*). *Cryptogam. Mycol.* **2000**, *21*, 147–152. [CrossRef]
12. Tejedor-Calvo, E.; García-Barreda, S.; Felices-Mayordomo, M.; Blanco, D.; Sánchez, S.; Marco, P. Truffle Flavored Commercial Products Veracity and Sensory Analysis from Truffle and Non-Truffle Consumers. *Food Control.* **2023**, *145*, 109424. [CrossRef]
13. Splivallo, R.; Valdez, N.; Kirchhoff, N.; Ona, M.C.; Schmidt, J.P.; Feussner, I.; Karlovsky, P. Intraspecific Genotypic Variability Determines Concentrations of Key Truffle Volatiles. *New Phytol.* **2012**, *194*, 823–835. [CrossRef] [PubMed]
14. Zarivi, O.; Cesare, P.; Ragnelli, A.M.; Aimola, P.; Leonardi, M.; Bonfigli, A.; Colafarina, S.; Poma, A.M.; Miranda, M.; Pacioni, G. Validation of Reference Genes for Quantitative Real-Time PCR in Périgord Black Truffle (*Tuber Melanosporum*) Developmental Stages. *Phytochemistry* **2015**, *116*, 78–86. [CrossRef] [PubMed]
15. Krösser, D.; Dreyer, B.; Siebels, B.; Voß, H.; Krisp, C.; Schlüter, H. Investigation of the Proteomes of the Truffles *Tuber Albidum Pico*, *T. aestivum*, *T. indicum*, *T. magnatum*, and *T. melanosporum*. *Int. J. Mol. Sci.* **2021**, *22*, 12999. [CrossRef] [PubMed]
16. Creydt, M.; Fischer, M. Food Authentication: Truffle Species Classification by Non-Targeted Lipidomics Analyses Using Mass Spectrometry Assisted by Ion Mobility Separation. *Mol. Omics* **2022**, *18*, 616–626. [CrossRef] [PubMed]
17. Losso, K.; Wörz, H.; Kappacher, C.; Huber, S.; Jakschitz, T.; Rainer, M.; Bonn, G.K. Rapid Quality Control of Black Truffles Using Direct Analysis in Real Time Mass Spectrometry and Hydrophilic Interaction Liquid Chromatography Mass Spectrometry. *Food Chem.* **2023**, *403*, 134418. [CrossRef]
18. Segelke, T.; Schelm, S.; Ahlers, C.; Fischer, M. Food Authentication: Truffle (*Tuber* spp.) Species Differentiation by FT-NIR and Chemometrics. *Foods* **2020**, *9*, 922. [CrossRef] [PubMed]
19. Segelke, T.; Von Wuthenau, K.; Neitzke, G.; Müller, M.S.; Fischer, M. Food Authentication: Species and Origin Determination of Truffles (*Tuber* spp.) by Inductively Coupled Plasma Mass Spectrometry and Chemometrics. *J. Agric. Food Chem.* **2020**, *68*, 14374–14385. [CrossRef]
20. Bligh, E.G.; Dyer, W.J. A Rapid Method of Total Lipid Extraction and Purification. *Can. J. Biochem. Physiol.* **1959**, *37*, 911–917. [CrossRef]
21. Reisdorph, R.; Michel, C.; Quinn, K.; Doenges, K.; Reisdorph, N. Untargeted Differential Metabolomics Analysis Using Drift Tube Ion Mobility-Mass Spectrometry. In *Ion Mobility-Mass Spectrometr: Methods and Protocolsy*; Humana: New York, NY, USA, 2020; pp. 55–78.
22. Poverenov, E.; Arnon-Rips, H.; Zaitsev, Y.; Bar, V.; Danay, O.; Horev, B.; Bilbao-Sainz, C.; McHugh, T.; Rodov, V. Potential of Chitosan from Mushroom Waste to Enhance Quality and Storability of Fresh-Cut Melons. *Food Chem.* **2018**, *268*, 233–241. [CrossRef]
23. Pacific Northwest National Laboratory PNNL Preprocessor Software. Available online: https://Pnnl-Comp-Mass-Spec.Github.Io/PNNL-PreProcessor (accessed on 1 April 2023).
24. Benjamini, Y.; Hochberg, Y. Controlling the False Discovery Rate: A Practical and Powerful Approach to Multiple Testing. *J. R. Stat. Soc. Ser. B Methodol.* **1995**, *57*, 289–300. [CrossRef]
25. Sud, M.; Fahy, E.; Cotter, D.; Brown, A.; Dennis, E.A.; Glass, C.K.; Merrill, A.H.; Murphy, R.C.; Raetz, C.R.H.; Russell, D.W.; et al. LMSD: LIPID MAPS Structure Database. *Nucleic Acids Res.* **2007**, *35*, D527–D532. [CrossRef] [PubMed]
26. FooDB. The Metabolomics Innovation Centre (TMIC). Available online: https://foodb.ca (accessed on 1 June 2023).
27. Zhou, Z.; Tu, J.; Xiong, X.; Shen, X.; Zhu, Z.-J. LipidCCS: Prediction of Collision Cross-Section Values for Lipids with High Precision to Support Ion Mobility–Mass Spectrometry-Based Lipidomics. *Anal. Chem.* **2017**, *89*, 9559–9566. [CrossRef] [PubMed]
28. Zhu Lab. Available online: https://www.zhulab.cn/LipidCCS/ (accessed on 1 June 2023).
29. Sumner, L.W.; Amberg, A.; Barrett, D.; Beale, M.H.; Beger, R.; Daykin, C.A.; Fan, T.W.-M.; Fiehn, O.; Goodacre, R.; Griffin, J.L.; et al. Proposed Minimum Reporting Standards for Chemical Analysis. *Metabolomics* **2007**, *3*, 211–221. [CrossRef] [PubMed]
30. Li, Y.; Lou, Y.; Mu, T.; Xu, J.; Zhou, C.; Yan, X. Simultaneous Structural Identification of Diacylglyceryl-*N*-trimethylhomoserine (DGTS) and Diacylglycerylhydroxymethyl-*N*,*N*,*N*-trimethyl-β-alanine (DGTA) in Microalgae Using Dual Li^+/H^+ Adduct Ion Mode by Ultra-performance Liquid Chromatography/Quadrupole Time-of-flight Mass Spectrometry. *Rapid Commun. Mass Spectrom.* **2017**, *31*, 457–468. [CrossRef] [PubMed]
31. PRIMe RIKEN Center for Sustainable Resource Science. 2023. Available online: https://metabography.riken.jp/menta.cgi/lipidomics/search_query_spectrum (accessed on 1 June 2023).
32. Sande, D.; de Oliveira, G.P.; Moura, M.A.F.E.; de Almeida Martins, B.; Lima, M.T.N.S.; Takahashi, J.A. Edible Mushrooms as a Ubiquitous Source of Essential Fatty Acids. *Food Res. Int.* **2019**, *125*, 108524. [CrossRef]
33. Brennan, P.J.; Griffin, P.F.S.; Lösel, D.M.; Tyrrell, D. The Lipids of Fungi. *Prog. Chem. Fats Other Lipids* **1975**, *14*, 49–89. [CrossRef] [PubMed]
34. Holtz, R.B.; Schisler, L.C. Lipid Metabolism of *Agaricus Bisporus* (Lange) Sing.: I. Analysis of Sporophore and Mycelial Lipids. *Lipids* **1971**, *6*, 176–180. [CrossRef]

35. Shin, J.-H.; Shon, J.C.; Lee, K.; Kim, S.; Park, C.S.; Choi, E.H.; Lee, C.H.; Lee, H.S.; Liu, K.-H. A Lipidomic Platform Establishment for Structural Identification of Skin Ceramides with Non-Hydroxyacyl Chains. *Anal. Bioanal. Chem.* **2014**, *406*, 1917–1932. [CrossRef]
36. Colby, S.M.; Nuñez, J.R.; Hodas, N.O.; Corley, C.D.; Renslow, R.R. Deep Learning to Generate in Silico Chemical Property Libraries and Candidate Molecules for Small Molecule Identification in Complex Samples. *Anal. Chem.* **2020**, *92*, 1720–1729. [CrossRef] [PubMed]
37. Zhou, Z.; Luo, M.; Chen, X.; Yin, Y.; Xiong, X.; Wang, R.; Zhu, Z.-J. Ion Mobility Collision Cross-Section Atlas for Known and Unknown Metabolite Annotation in Untargeted Metabolomics. *Nat. Commun.* **2020**, *11*, 4334. [CrossRef]
38. Plante, P.-L.; Francovic-Fontaine, É.; May, J.C.; McLean, J.A.; Baker, E.S.; Laviolette, F.; Marchand, M.; Corbeil, J. Predicting Ion Mobility Collision Cross-Sections Using a Deep Neural Network: DeepCCS. *Anal. Chem.* **2019**, *91*, 5191–5199. [CrossRef] [PubMed]
39. Warnecke, D.; Heinz, E. Recently Discovered Functions of Glucosylceramides in Plants and Fungi. *Cell. Mol. Life Sci.* **2003**, *60*, 919–941. [CrossRef] [PubMed]
40. McAnoy, A.M.; Wu, C.C.; Murphy, R.C. Direct Qualitative Analysis of Triacylglycerols by Electrospray Mass Spectrometry Using a Linear Ion Trap. *J. Am. Soc. Mass Spectrom.* **2005**, *16*, 1498–1509. [CrossRef]
41. Eichmann, T.O.; Lass, A. DAG Tales: The Multiple Faces of Diacylglycerol—Stereochemistry, Metabolism, and Signaling. *Cell. Mol. Life Sci.* **2015**, *72*, 3931–3952. [CrossRef] [PubMed]
42. Splivallo, R.; Ottonello, S.; Mello, A.; Karlovsky, P. Truffle Volatiles: From Chemical Ecology to Aroma Biosynthesis. *New Phytol.* **2011**, *189*, 688–699. [CrossRef] [PubMed]
43. Tejedor-Calvo, E.; Marco, P.; Spègel, P.; Soler-Rivas, C. Extraction and Trapping of Truffle Flavoring Compounds into Food Matrices Using Supercritical CO_2. *Food Res. Int.* **2023**, *164*, 112422. [CrossRef] [PubMed]
44. Gao, J.-M.; Zhang, A.-L.; Chen, H.; Liu, J.-K. Molecular Species of Ceramides from the Ascomycete Truffle *Tuber indicum*. *Chem. Phys. Lipids* **2004**, *131*, 205–213. [CrossRef]
45. Gao, J.-M.; Zhu, W.-M.; Zhang, S.-Q.; Zhang, X.; Zhang, A.-L.; Chen, H.; Sun, Y.-Y.; Tang, M. Sphingolipids from the Edible Fungus *Tuber indicum*. *Eur. J. Lipid Sci. Technol.* **2004**, *106*, 815–821. [CrossRef]
46. United Nations. *Unece Standard FFV-53*, 2017th ed.; United Nations: New York, NY, USA; Geneva, Switzerland, 2017.
47. Tejedor-Calvo, E.; Garcia-Barreda, S.; Sebastián Dambolena, J.; Pelissero, D.; Sánchez, S.; Marco, P.; Nouhra, E. Aromatic Profile of Black Truffle Grown in Argentina: Characterization of Commercial Categories and Alterations Associated to Maturation, Harvesting Date and Orchard Management Practices. *Food Res. Int.* **2023**, *173*, 113300. [CrossRef]
48. Niimi, J.; Deveau, A.; Splivallo, R. Geographical-based Variations in White Truffle Tuber Magnatum Aroma Is Explained by Quantitative Differences in Key Volatile Compounds. *New Phytol.* **2021**, *230*, 1623–1638. [CrossRef]
49. Strojnik, L.; Grebenc, T.; Ogrinc, N. Species and Geographic Variability in Truffle Aromas. *Food Chem. Toxicol.* **2020**, *142*, 111434. [CrossRef] [PubMed]
50. Gioacchini, A.M.; Menotta, M.; Guescini, M.; Saltarelli, R.; Ceccaroli, P.; Amicucci, A.; Barbieri, E.; Giomaro, G.; Stocchi, V. Geographical Traceability of Italian White Truffle (*Tuber Magnatum* Pico) by the Analysis of Volatile Organic Compounds. *Rapid Commun. Mass Spectrom.* **2008**, *22*, 3147–3153. [CrossRef] [PubMed]
51. Šiškovič, N.; Strojnik, L.; Grebenc, T.; Vidrih, R.; Ogrinc, N. Differentiation between Species and Regional Origin of Fresh and Freeze-Dried Truffles According to Their Volatile Profiles. *Food Control* **2021**, *123*, 107698. [CrossRef]
52. Tejedor-Calvo, E.; Morales, D.; Marco, P.; Sánchez, S.; Garcia-Barreda, S.; Smiderle, F.R.; Iacomini, M.; Villalva, M.; Santoyo, S.; Soler-Rivas, C. Screening of Bioactive Compounds in Truffles and Evaluation of Pressurized Liquid Extractions (PLE) to Obtain Fractions with Biological Activities. *Food Res. Int.* **2020**, *132*, 109054. [CrossRef] [PubMed]

Disclaimer/Publisher's Note: The statements, opinions and data contained in all publications are solely those of the individual author(s) and contributor(s) and not of MDPI and/or the editor(s). MDPI and/or the editor(s) disclaim responsibility for any injury to people or property resulting from any ideas, methods, instructions or products referred to in the content.